Propagating and Standing Components of the Intraseasonal Oscillation in Tropical Convection

CHIDONG ZHANG

Department of Atmospheric Sciences and Joint Institute for the Study of the Atmosphere and Ocean, University of Washington, Seattle, Washington

HARRY H. HENDON

Cooperative Institute for Research in Environmental Sciences, University of Colorado, Boulder, Colorado

(Manuscript received 4 September 1995, in final form 11 June 1996)

ABSTRACT

Two questions related to the intraseasonal variability of tropical convection and circulation remain controversial. 1) To what degree is the convective component of the Madden–Julian oscillation (MJO) a standing oscillation? 2) Is the eastward propagating circulation anomaly of the MJO coherent with a standing oscillation in convection?

In an attempt to settle these issues, the authors undertake a series of statistical analyses of gridded outgoing longwave radiation and winds to quantify the magnitudes of the propagating and standing components of convection and their coherence with the propagating component of the circulation. They demonstrate that no dominant standing oscillation in convection can be identified. Instead, intraseasonal variability of convection is dominated by an eastward propagating mode, which the authors interpret as the convective signal of the MJO. This propagating component accounts for almost all of the convective variance that is coherent with the eastward propagating disturbance in the zonal wind, which is a traditional measure of the MJO. Analysis of synthetic time series illustrates that an impression of a standing oscillation in convection may come forth because of the modulation of the eastward propagating convective disturbance by an amplitude envelope with maxima in the eastern Indian and western Pacific Oceans and a minimum over the maritime continents.

1. Introduction

Intraseasonal variability within the equatorial troposphere is characterized by a preponderance of eastward propagating, planetary-scale disturbances in zonal wind (e.g., Hayashi and Golder 1986) and convection (e.g., Nakazawa 1986). The phenomenon associated with the broad spectral peak centered on 50 days for eastward wavenumbers 1–3 (e.g., Salby and Hendon 1994) is commonly referred to as the Madden–Julian oscillation (MJO; Madden and Julian 1971, 1972). The signal of the MJO (i.e., a spectral peak at eastward, planetary-scale wavenumbers) is significant typically during boreal winter (e.g., Salby and Hendon 1994). Intraseasonal variability of winds and convection during boreal summer, while locally exhibiting spectral peaks over the Indian Ocean and southeast Asia, does not exhibit pronounced eastward propagation along the equator (e.g., Rui and Wang 1990) and, hence, is not referred to here as the MJO.

The circulation anomaly associated with the eastward propagating MJO is coupled to anomalous convection across the Indian and western Pacific Oceans. Together they move eastward at 3–5 m s^{-1} and exhibit a local period of about 50 days. The anomalies in convection and low-level (e.g., 850 hPa) wind are observed to decay east of the date line. There, the phase speed of the upper-level (e.g., 200 hPa) circulation anomaly increases to greater than 10 m s^{-1} (e.g., Madden and Julian 1972; Weickmann et al. 1985; Hendon and Salby 1994).

Many theoretical and numerical modeling studies have been devoted to understanding the mechanism of the MJO. Cooperative interaction between convection and circulation is generally regarded as the main mechanism of the MJO. Feedback between convection and circulation induced by large-scale moisture convergence (e.g., Lau and Peng 1987; Wang 1988; Salby et al. 1994) and by surface turbulent fluxes of heat and moisture (Emanuel 1987; Neelin et al. 1987) are two such mechanisms.

Contradictory to the hypothesis that the MJO results from cooperative interaction between convection and circulation is the notion that the MJO consists mainly of an eastward propagating disturbance in the zonal

Corresponding author address: Dr. Chidong Zhang, University of Washington, JISAO, Box 354235, Seattle, WA 98195-4235.
E-mail: chidong@atmos.washington.edu

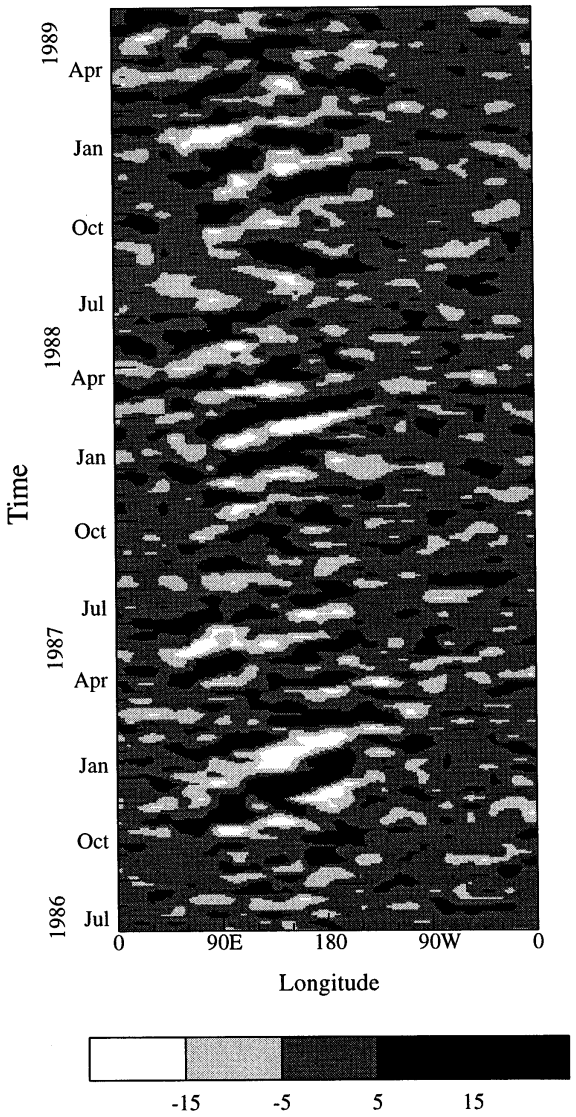

FIG. 1. Time–longitude diagram for anomalous OLR (W m^{-2}) averaged between 20°N and 20°S for 1 July 1986–30 June 1989. Further description of the OLR data is given in section 2.

wind that radiates away from a localized standing oscillation in convection (e.g., Yamagata and Hayashi 1984). This latter hypothesis appears to be supported by observations that seemingly indicate that convection associated with the MJO possesses a significant standing component, whose centers of action are in the eastern Indian and western Pacific Oceans (e.g., Lau and Chan 1985; Hsu et al. 1990; Weickmann and Khalsa 1990; Zhu and Wang 1993). Figure 1 displays a typical example of the time–longitude behavior of anomalous outgoing longwave radiation (OLR; described in section 2) in the equatorial region for the period 1 July 1986 through 30 June 1989. The phenomenon of eastward propagation is easy to identify, although the signal is confined in longitude (mainly between 30° and 240°E) and its strength depends on the season (stronger in boreal winters) as well as longitude (stronger near 90°E and 180°). Standing oscillations seem to exist at various longitudes and time. For example, localized standing oscillations at 90°E are apparent during March–June 1987.

This impression of a lack of continuous eastward propagation of convection, based on viewing figures such as Fig. 1, has led to some speculation that the eastward propagating disturbance in the circulation develops independently of an eastward propagating convective disturbance. The postulated mechanisms include intrusions of extratropical perturbations into the Tropics (Hsu et al. 1990) and radiation of dynamical disturbances away from localized, stochastic convective heating (Salby and Garcia 1987). While the production of a spectral peak near 50 days in the dynamical disturbances is not dependent on a similar spectral peak in convection for the latter mechanism, numerical simulations suggest that local interactions between convection, evaporation, and radiation can produce a local standing oscillation in convection with a near 50-day period (Hu and Randall 1994). Motivated by the possibility that intraseasonal perturbations in circulation are induced by standing oscillations in convection, numerical simulations have been conducted in which spatially confined, stationary forcing oscillating with a given frequency is prescribed to stimulate intraseasonal perturbations in circulation (e.g., Yamagata and Hayashi 1984; Anderson and Stevens 1987). However, such simulations typically fail to capture eastward propagation of the subtropical Rossby gyres, which accompany the convective anomaly as it traverses the Eastern Hemisphere (Hendon and Salby 1994).

There appears to be little dispute that strong intraseasonal oscillations of tropical convection are mainly confined to the Eastern Hemisphere, where the signal of the MJO in the circulation of the Western Hemisphere primarily originates. The question remains unsettled, however, whether the MJO consists of or results from a prominent standing convective component and whether the disturbance in the wind field is dynamically coupled to the convective disturbance *in the Eastern Hemisphere*. Based on existing observational, theoretical, and numerical studies, three mechanistic scenarios for the MJO are suggested.

1) The MJO is a phenomenon of mutual eastward propagation in both convection and circulation; interactions between the disturbances in convection and circulation are vital to the existence and eastward propagation of the MJO itself.
2) The MJO is mainly an eastward propagating disturbance in the circulation induced by a localized standing oscillation in convection with a particular period (e.g., 50-day period).
3) The MJO is primarily an eastward propagating disturbance in the circulation induced by stochastic con-

vective activity fluctuating with no predominant space or timescale.

The possibility that a standing component of convection is generated by a spatial modulation of a purely eastward propagating disturbance (e.g., Rui and Wang 1990; Hayashi and Golder 1986; Salby and Hendon 1994) is permitted under scenario 1. In scenarios 2 and 3, eastward propagating convective disturbances may exist, but not as a driving mechanism of the MJO; they merely are consequences of the modulation of convection by the eastward propagating disturbance in the circulation.

These three scenarios pose very different dynamical frameworks for understanding how large-scale convection and circulation interact on intraseasonal timescales. It is therefore useful to directly compare and evaluate them based on observations, theories, and numerical simulations. Evaluating these three scenarios is in turn very important to how observational, theoretical, and numerical studies of the MJO should be pursued. Key aspects for evaluating the three scenarios can be obtained from observations. For example, whether the intraseasonal variability of convection is dominated by standing oscillations helps to determine if scenario 2 is likely to be valid or should be ruled out. Scenario 1 would be favored over scenario 2 provided, in the absence of a strong signal of standing oscillation, eastward propagating signals dominate the intraseasonal variability of convection and are strongly coherent in both time and space with the eastward propagating disturbance in circulation.

In the present study, we attempt to clarify to what degree the convective component of the MJO can be characterized as a standing oscillation from which the disturbance in the circulation emanates and to what degree the convective component is a propagating phenomenon, which is coupled to the eastward propagating disturbance in the circulation. Specifically, we attempt to provide some statistical evidence that is useful for judging the three proposed scenarios. We use OLR and wind analyses from the European Centre for Medium-Range Weather Forecasts (ECMWF) to represent large-scale variability in tropical convection and circulation, respectively. Propagating and standing signals in these two datasets and their coherence are identified using statistical analyses, including space–time spectrum analysis, empirical orthogonal function analysis (EOF), and singular value decomposition analysis (SVD). The data and analysis methods are described in section 2. Results of the statistical analyses are presented in section 3. A summary and discussions are given in section 4, where synthetic time series are constructed and analyzed to interpret the results based on OLR and ECMWF winds.

2. Data and methods

Daily mean OLR, which serves as a proxy for large-scale convective activity, and daily mean zonal winds at 850 hPa from ECMWF analyses are used for the period 1 July 1986–31 December 1993. As the signal of the MJO in convection has been previously identified to be at eastward wavenumbers less than 4 with periods of 30–90 days (e.g., Nakazawa 1986; Salby and Hendon 1994), analyses here will be based on intraseasonally filtered data that captures this broad range of periods and wavenumbers. The temporal filter is formed by subtracting a 91-day running mean from the data and then applying a 5-day mean. Low- (periods $>$ 180 days) and high- (periods $<$ 10 days) frequency variability is thus removed. Intraseasonal signals identified with spectral, EOF, and SVD analyses are not sensitive to the characteristics of this broad filtering. The large spatial scale of the MJO is emphasized by averaging the pentadal time series over grid boxes of 10° longitude by 5° latitude. Time series of this temporally and spatially filtered data are denoted with primes (i.e., OLR′ and U'_{850}). Table 1 lists these and other symbols used in this study.

TABLE 1. Symbols used in this study.

Symbol	Definition
OLR′	Pentad-mean anomalous OLR time series
OLR'_p	Propogating component of OLR′, i.e., reconstructed time series based on the first two eigenmodes from HSVD analysis of OLR′
OLR'_{np}	Nonpropagating component of OLR′, i.e., $\mathrm{OLR}'_{np} = \mathrm{OLR}' - \mathrm{OLR}'_p$
OLR*	Reconstructed OLR time series based on the first two eigenmodes from SVD analysis of OLR′ and U'_{850}
δOLR′	Residual time series of OLR′, i.e., $\delta\mathrm{OLR}' = \mathrm{OLR}' - \mathrm{OLR}^*$
U'_{850}	Pentad-mean anomalous time series of the zonal wind at 850 hPa
U^*_{850}	Reconstructed time series of the zonal wind at 850 hPa based on the first two eigenmodes from SVD analysis of OLR′ and U'_{850}
$\delta U'_{850}$	Residual time series of the zonal wind at 850 hPa, i.e., $\delta U'_{850} = U'_{850} - U^*_{850}$

EOF analysis is a powerful tool for identifying coherent patterns that explain the largest fraction of the total variance of a field and has been used extensively in studies of intraseasonal variations in tropical convection (e.g., Knutson and Weickmann 1987; Lau and Chan 1988). A single eigenmode from EOF analysis represents a standing oscillation; propagating disturbances are represented by pairs of modes whose principal components are temporally in quadrature. SVD analysis (Bretherton et al. 1992; Wallace et al. 1992) is useful for identifying coherent patterns between two fields. SVD analysis can also be applied directly to a field and its temporal tendency. In the latter case, a propagating component of a field would be represented by a pair of eigenmodes in quadrature with each other in time and space, while a standing component cannot be represented by any single or group of eigenmodes. A general way to calculate the tendency is via the Hilbert

transform (Barnett 1983). Hereafter, we will refer to HSVD as SVD analysis applied to a field and its Hilbert transform.

A critical issue in using EOF or SVD analysis is whether a particular eigenmode by itself bears any physical meaning and, therefore, whether it is justifiable to discuss the features of this mode in isolation from other eigenmodes. With regard to this issue, we adopt a separation criterion suggested by North et al. (1982). According to this criterion, an eigenmode n can be taken as a physically meaningful identity only when the corresponding eigenvalue λ_n is well separated from the neighboring ones; that is,

$$\delta\lambda_{n-1} < \Delta\lambda_{n-1} \text{ and } \delta\lambda_n < \Delta\lambda_n, \tag{1}$$

where

$$\delta\lambda_n = \lambda_n(2/L)^{1/2} \tag{2}$$

is the sampling error of λ_n, $\Delta\lambda_n = \lambda_n - \lambda_{n+1}$ is the eigenvalue increment, and L is the estimated effective number of degrees of freedom. If two adjacent eigenvalues are not well separated from each other but together are well separated from their neighboring eigenvalues, that is, if $\delta\lambda_n \geq \Delta\lambda_n$ but $\delta\lambda_{n-1} < \Delta\lambda_{n-1}$ and $\delta\lambda_{n+1} < \Delta\lambda_{n+1}$, then the corresponding two eigenmodes (n and $n+1$) as a pair may be combined to represent a physically meaningful pattern. We will hereafter use the term ''outstanding'' to describe single or pairs of eigenmodes that are well separated from others based on criterion (1). The number of degrees of freedom L in (2) is estimated as the total number of data samples (i.e., the total number of pentads in a time series) divided by 12 (the number of pentads for a 60-day period) for EOF and SVD analyses and divided by 24 for HSVD analyses.

Power spectra of the intraseasonally filtered input fields and of fields reconstructed from dominant eigenmodes are computed for latitudinal means of the pentadal time series between 7.5°N and 7.5°S. This range of latitudes is where the planetary-scale, eastward propagating signal of the MJO is concentrated (e.g., Salby and Hendon 1994). The frequency wavenumber spectrum is computed by Fourier transform technique. Raw spectral estimates, with nominal bandwidth of 4.24×10^{-4} cycles per day, are smoothed with 10 passes of a three-point running average, which yields an effective bandwidth of 2.4×10^{-3} cycles per day.

The goal of this study is to quantify the degree to which the signal of the MJO in convection can be considered to be a standing oscillation. Standing oscillations are defined (e.g., Hayashi 1979) as transient waves with their nodes fixed in space. Standing oscillations can be viewed as a pair of waves of the same wavenumber, frequency, and amplitude but propagating in opposite directions. Let $E(k, \omega)$ be the variance associated with an eastward component at frequency ω and wavenumber k. Then $E(k,-\omega)$ is the variance associated with the westward component at frequency ω and wavenumber k. Following Pratt (1976), if the eastward variance exceeds the westward variance, then an eastward propagating fluctuation is indicated with variance equal to the difference of the eastward and westward variances. All or part of the remaining variance (in this case equal to twice the westward variance) may be associated with a standing component, depending on the temporal coherence between the eastward and westward components. For a single wavenumber and frequency, the coherence is identically one. In practice, however, the phenomenon of interests spans a range of frequencies and wavenumbers, resulting from transience and spatial localization. Hence, the coherence is generally less than one (e.g., Pratt 1976). Here, we will only identify the most optimistic estimate of the standing variance [i.e., equal to twice the lesser of $E(k, \omega)$ and $E(k,-\omega)$, where k and ω now indicate a range of wavenumbers and frequencies].

By considering together the results of EOF, SVD, and space-time spectral analyses, we expect–

1) a single outstanding EOF eigenmode of OLR′, with which the reconstructed OLR time series shows equal eastward and westward moving power at planetary spatial scales (zonal wavenumber $k = 1$–3) and intraseasonal timescales (periods 35–90 days), if the intraseasonal oscillation in convection consists of a dominant standing component;
2) an outstanding pair of eigenmodes in quadrature with each other from EOF and HSVD analyses of OLR′, with which the reconstructed OLR time series shows dominant eastward moving power at planetary spatial scales and intraseasonal timescales, if the intraseasonal oscillation in convection consists of a significant propagating component;
3) outstanding eigenmodes from SVD analysis for OLR′ and U'_{850}, demonstrating strong coherence between the standing component of OLR, if it exists, with propagating components in U'_{850}, if scenario 2 is correct;[1] and
4) outstanding eigenmodes from SVD analysis for OLR′ and U'_{850}, demonstrating strong coherence between the propagating component of OLR′, if it exists in the absence of a standing oscillation in convection, and propagating components in U'_{850}, if either scenarios 1 or 3 are correct. In this case, these two scenarios cannot be distinguished from each other based on the analyses used in this study but preference can be made based on other information.

[1] When a standing component of OLR is coherent with a propagating component of U_{850}, SVD would result in an outstanding single, not paired, mode that represents the standing component of OLR and only part of the propagating component of U_{850}.

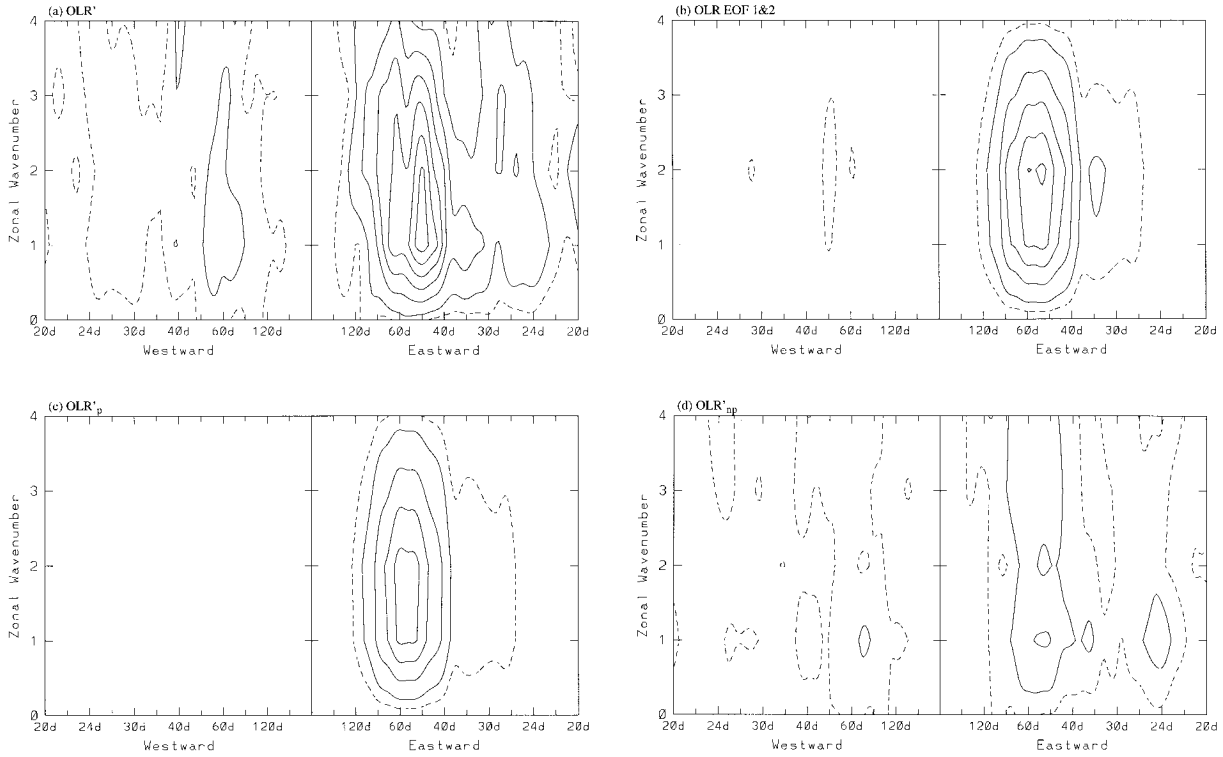

FIG. 2. Space–time power spectra for (a) OLR′, (b) OLR reconstructed from the first two modes of EOF analysis for OLR′, (c) OLR'_p, and (d) OLR'_{np}. Contour interval is 9×10^{-2} W^2 m^{-4}, with the dashed line at 4.5×10^{-2} W^2 m^{-4}.

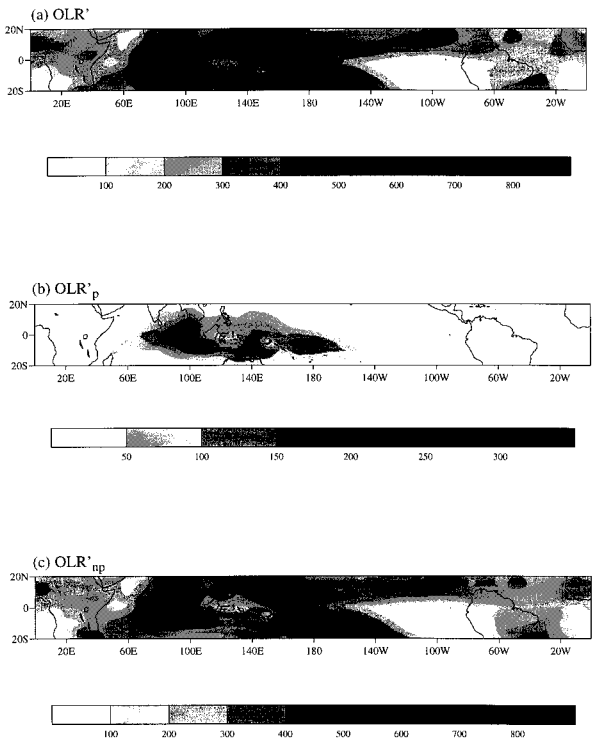

FIG. 3. Variance of (a) OLR′, (b) OLR'_p, and (c) OLR'_{np} (W^2 m^{-4}).

3. Results

a. General features of OLR

The space–time power spectrum for OLR′ is shown in Fig. 2a. The abscissa is linear in frequency but is labeled in equivalent period. The spectrum is highly asymmetric with eastward variance swamping westward variance. A broad spectral peak occurs for eastward wavenumbers 1–3 with period near 50 days [see also Salby and Hendon (1994), who display a similarly computed spectrum but for the period 1979–89]. The ratio of variance for eastward to westward components at $k = 1$–3 and $\tau = 35$–90 days is 4 to 1. This suggests that the standing variance is at most two-thirds of the eastward propagating variance, if twice the westward variance for wavenumbers 1–3 and periods 35–90 days can be regarded as standing variance [as discussed by Pratt (1976), this is probably an overestimate].

The spatial distribution of variance of OLR′ is shown in Fig. 3a. Large variance is found in regions of climatological convection, including the eastern Indian and western Pacific Oceans, the South Pacific convergence zone (SPCZ), and the eastern Pacific intertropical convergence zone (ITCZ). Maximum variance occurs in the eastern Indian and western Pacific Oceans where the convective variability associated with the MJO is the strongest (e.g., Salby and Hendon 1994). While large variance in the ITCZ and SPCZ is a feature of boreal

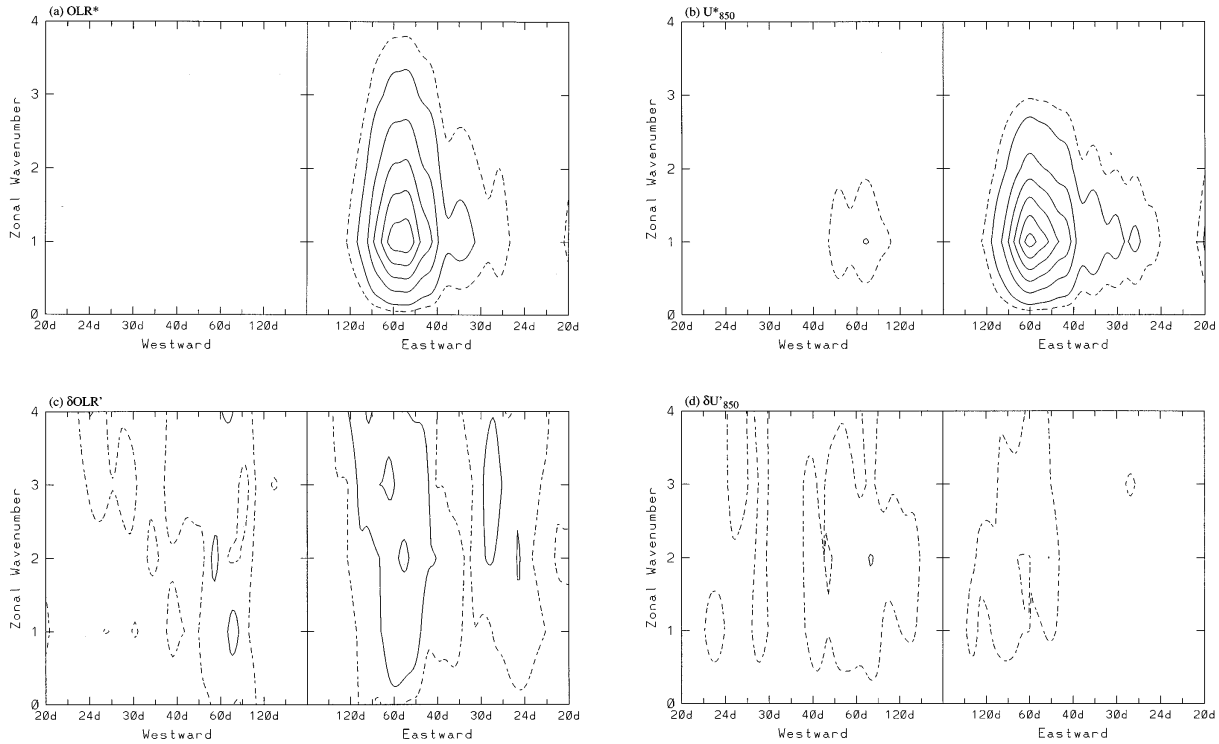

FIG. 4. Space–time power spectra for (a) OLR*, (b) U^*_{850}, (c) δOLR′, and (d) $\delta U'_{850}$. Contour interval in (a) and (c) is as in Fig. 2. Contour interval in (b) and (d) is 3.5×10^{-3} m^2 s^{-2}, with the dashed line at 1.75×10^{-3} m^2 s^{-2}.

summer and winter, respectively, large variance in the equatorial eastern Indian Ocean emerges in both seasons (see also Fig. 4 of Lau and Chan 1985). It is especially noticeable that the variance is relatively small over the Maritime Continent. Zhu and Wang (1993) have shown evidence of a seesaw in convection between the regions of maximum intraseasonal variance in the eastern Indian and western Pacific Oceans, with the node located over the Maritime Continent. As discussed in section 1, the eastern Indian Ocean is where a standing oscillation in convection seems to be prominent (Fig. 1).

b. EOF analysis of OLR′

The EOF analysis applied to OLR′ does not result in any single outstanding eigenmode. Instead, the only outstanding modes are the first two as a pair (Table 2). The principal components of these two modes are temporally quadrature, indicating that they collectively describe a spatially propagating mode (see also Lau and Chan 1988). The space–time power spectrum of OLR reconstructed from these two modes shows a highly asymmetric distribution with eastward variance dominating over westward variance (Fig. 2b). Maximum power occurs at eastward wavenumbers 1 and 2 and $\tau = 50$–60 days, but significant power occurs in wavenumber 3 as well. The ratio between the eastward and westward power at $k = 1$–3 and $\tau = 35$–90 days is about 8 to 1, which suggests that the standing component is at least 3.5 times smaller than the eastward propagating component. Taken together, these results strongly imply that the dominant mode of intraseasonal convective activity (i.e., the convective manifestation of the MJO) is predominantly an eastward propagating disturbance.

TABLE 2. Eigenvalues (λ_n) and their sampling errors ($\delta\lambda_n$) and increments ($\delta\lambda_n$) of the first six eigenmodes from EOF analysis of OLR′.

n	1	2	3	4	5	6
λ_n	18.3	15.7	10.97	9.0	8.3	7.6
$\delta\lambda_n$	4.0	3.4	2.4	2.0	1.8	1.7
$\Delta\lambda_n$	2.6	4.8	2.0	0.7	0.6	0.7

c. HSVD analysis of OLR′

HSVD analysis of OLR′ yields a pair of outstanding eigenmodes (Table 3). Correlation between the expan-

TABLE 3. Eigenvalues (λ_n), their sampling errors ($\delta\lambda_n$) and increments ($\lambda\lambda_n$), and correlation coefficients (Cr) between the expansion coefficients of the left and right fields of the first six eigenmodes from HSVD analysis of OLR′.

n	1	2	3	4	5	6
λ_n	12.6	12.6	5.5	5.5	4.7	4.7
$\delta\lambda_n$	3.9	3.9	1.7	1.7	1.4	1.4
$\Delta\lambda_n$	0.0	7.1	0.0	0.7	0.0	1.4
Cr	0.79	0.79	0.68	0.68	0.66	0.66

sion coefficients of the left and right fields is very high (0.8) for these first two modes. As for the leading two modes from the EOF analysis, these two HSVD modes are in quadrature in longitude as well as in time, indicating that they describe a zonally propagating mode. The time series of OLR reconstructed from these two modes is referred to as the propagating component of OLR, denoted by OLR'_p. This designation does not imply that there are no other propagating components of intraseasonal convective activity. Rather, it indicates that the dominant mode of intraseasonal convective variance is, as will be shown below, predominantly eastward propagating. The space–time power spectrum of OLR'_p (Fig. 2c) is very similar to that from the leading two EOFs (Fig. 2b), except here the westward power is even weaker. The ratio between eastward and westward power at $k = 1$–3 and $\tau = 35$–90 days is about 15 to 1. Hence, the HSVD analysis more effectively discriminates to the eastward propagating components than does the EOF analysis. The spatial distribution of variance of OLR'_p is highly concentrated in the equatorial region from 70°–200°E (Fig. 3b). Maximum variance is located in the eastern Indian and western Pacific Oceans, where the maximum variance of OLR′ is found (Fig. 3a). Similar distribution of the signal of convective variability associated with the MJO has been found by Salby and Hendon (1994) using different analyses.

The distribution of variance associated with OLR'_p (Fig. 3b) also bears resemblance to the distribution of intraseasonal variance of convection in the boreal winter shown by Lau and Chan (1988). This suggests that the variance during boreal winter results predominantly from eastward propagating components, which is also consistent with analyses by Salby and Hendon (1994). They show that the signal of eastward propagating variance at wavenumbers 1–3 is more prominent in boreal winter than in the summer. This seasonality of OLR'_p is apparent from the time series of the HSVD expansion coefficients and the time series of variance of OLR'_p, averaged over an 80-day running window and over longitudes 90°–180°E. Both time series show distinctly larger amplitudes in boreal winter than in summer (not shown).

Apart from the first two eigenmodes, no other outstanding mode(s) can be found from the HSVD analysis of OLR. We will refer to the difference between OLR′ and OLR'_p, that is, OLR′ - OLR'_p, as the nonpropagating component of OLR′, denoted by OLR'_{np}. Note that we have not referred to it as the standing component. Compared to OLR'_p, the variance of OLR'_{np} is more uniformly distributed across the Tropics (Fig. 3c). The local maxima in the eastern Indian and western Pacific Oceans are substantially reduced in comparison with those of OLR′. These maxima are no longer greater than the variance in other regions, such as southeast Asia, northeast of the Philippines, and the eastern Pacific ITCZ; these latter regions are not associated with strong signals of the MJO (Salby and Hendon 1994). In contrast to the spectrum of OLR'_p (Fig. 2c), the spectrum of OLR'_{np} (Fig. 2d) is bland, with no obvious spectral peak at westward or eastward wavenumbers and no obvious indication of a dominant standing component (i.e., equal power at eastward and westward periods for the same wavenumber). This lack of a dominant standing mode is confirmed by performing EOF analyses on OLR'_{np}: no outstanding eigenmode is found. Therefore, the HSVD analysis of OLR′ reveals that intraseasonal variability of tropical convection is dominated by an eastward propagating mode at wavenumbers 1–3 (i.e., OLR'_p), which we interpret as the convective signal of the MJO. The remaining variance at planetary scales exhibits no preferred direction of propagation or spatial or temporal scale.

TABLE 4. Eigenvalues (λ_n), their sampling errors ($\delta\lambda_n$) and increments ($\Delta\lambda_n$), and correlation coefficients (Cr) between the expansion coefficients of the left and right fields of the first six eigenmodes from SVD analysis of OLR′ and U'_{850}.

n	1	2	3	4	5	6
λ_n	15.3	12.6	7.0	6.5	5.6	4.6
$\delta\lambda_n$	3.4	2.8	1.6	1.5	1.3	1.0
$\Delta\lambda_n$	2.7	5.6	0.5	0.9	1.0	0.1
Cr	0.77	0.69	0.61	0.59	0.60	0.59

d. SVD analysis of OLR′ and U'_{850}

The only outstanding modes from the SVD analysis for OLR′ and U'_{850} are the first two as a pair (Table 4). The correlation between the expansion coefficients of the two variables is the highest for these two modes. Again, these two modes are in quadrature in longitude as well as in time. Reconstructed time series of OLR and 850-hPa zonal wind based on the first two SVD modes are denoted as OLR* and U^*_{850}, respectively. Their space–time power spectra are shown in Figs. 4a and 4b. Both show obvious dominance of eastward moving power at wavenumbers 1–3 for periods 35–90 days. The ratio between the eastward and westward power at $k = 1$–3 and $\tau = 35$–90 days is about 12 to 1 for OLR* and 6 to 1 for U^*_{850}.

The variance associated with U^*_{850} is sharply concentrated at wavenumber 1 (see also Salby and Hendon 1994, their Fig. 10). This is in contrast to that of OLR′, OLR reconstructed from EOFs 1 and 2, and OLR'_p, which is spread over wavenumbers 1–3. Salby and Hendon (1994) interpreted this contrasting behavior to indicate that the dynamical component of the MJO is more zonally extensive than the convective component. They further deduced that the concentration of convective power in the same frequency band (i.e., near 50-day period) for different wavenumbers results from a convective disturbance propagating through a variance envelope with maxima in the Indian and western Pacific Oceans. It is interesting to note that OLR* is more concentrated at wavenumber 1 than is OLR'_p or OLR re-

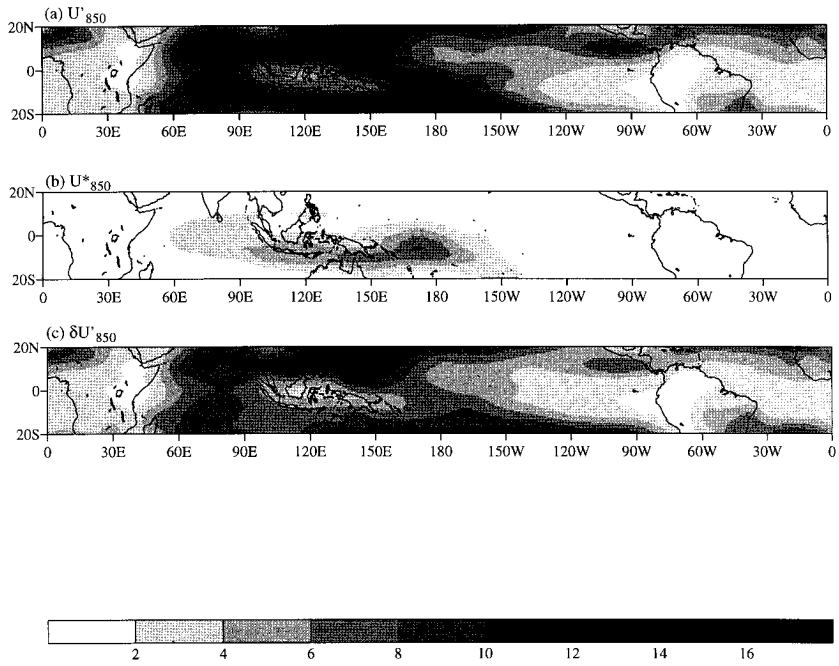

FIG. 5. Variance of (a) U', (b) U^*_{850}, and (c) $\delta U'_{850}$ (m^2 s^{-2}).

constructed from EOFs 1 and 2. This suggests that the circulation is related more closely to the broad-scale features of convection than to its amplitude modulation in longitude.

Distributions of the variance of U'_{850} and U^*_{850} are compared in Figs. 5a and 5b. Here, U'_{850} shows interesting minimum variance over the Maritime Continent. The variance of U^*_{850} is concentrated in the equatorial regions between 60°E and 140°W, with a maximum in the western Pacific (Fig. 5b). The region of largest variance is elongated in longitude from the eastern Indian Ocean to the western Pacific Ocean. This feature of off-equatorial maximum variance in U^*_{850} needs to be reconciled with mainstream theories for the MJO, in which the equatorial Kelvin wave, symmetric about the equator, serves as the dominant component of the MJO (e.g., Lau and Peng 1987; Wang 1988).

An HSVD analysis is also applied to U'_{850} in order to identify the dominant modes of intraseasonal variability in the zonal wind without regard to OLR. The resulting first two outstanding modes possess a spectrum and variance distribution that are essentially the same as those for U^*_{850}. We therefore conclude that most of the variance associated with the dominant eastward propagating mode of intraseasonally varying zonal wind at 850 hPa is captured by U^*_{850} and we thus interpret U^*_{850} as the signal of the MJO in the zonal wind at 850 hPa.

The spatial distribution of variance of OLR* is basically the same as that of OLR'_p (not shown). The time series of variance averaged over an 80-day running window and over longitudes 90°–180°E for OLR* is almost identical to that for OLR'_p (not shown). These indicate that OLR'_p accounts for almost all of the convective variance that is coherent with the eastward propagating circulation perturbation of the MJO.

A residual time series of OLR can be defined as $\delta\text{OLR}' = \text{OLR}' - \text{OLR}^*$. Similarly, a residual time series of 850-hPa zonal wind is defined as $\delta U'_{850} = U'_{850} - U^*_{850}$. The space–time spectra of $\delta\text{OLR}'$ and $\delta\text{U}'_{850}$ are shown in Figs. 4c and 4d, respectively. A lack of dominant eastward power for $\delta U'_{850}$ is obvious in Fig. 4d. In comparison, $\delta\text{OLR}'$ exhibits some increased eastward power at $\tau = 50$–60 days for $k = 3$. The ratio between the eastward and westward power at $k = 1$–3 and $\tau = 35$–90 days is 2 to 1 for $\delta\text{OLR}'$ and is 1.4 to 1 for $\delta U'_{850}$. This indicates that not all of the eastward propagating components of convection, especially for $k = 3$, are coherent with the eastward propagating components of the wind field. A common feature in Figs. 4c and 4d is that the power of these residual time series is distributed over a much wider range of spatial and temporal scales than that of OLR* and U^*_{850} (Figs. 4a and 4b). Figure 5c shows that the variance of $\delta U'_{850}$ is larger away from the equator than in the equatorial regions of the eastern Indian Ocean, the Maritime Continent, and the western Pacific Ocean, where the signals of the MJO are the strongest (Salby and Hendon 1994). The spatial distribution of variance for $\delta\text{OLR}'$ is similar to that for OLR'_{np}.

To further demonstrate that the only mode of U_{850} that is coherent with OLR is that which we associate with the eastward propagating MJO, SVD analyses are performed for OLR'_{np} with U'_{850} and for $\delta\text{OLR}'$ with U'_{850}.

TABLE 5. Eigenvalues (λ_n), their sampling errors ($\delta\lambda_n$) and increments ($\Delta\lambda_n$), and correlation coefficients (Cr) between the expansion coefficients of the left and right fields of the first six eigenmodes from SVD analysis of OLR'_{np} and U'_{850}.

n	1	2	3	4	5	6
λ_n	7.6	7.1	6.8	5.6	4.6	4.3
$\delta\lambda_n$	1.7	1.6	1.5	1.3	1.0	1.0
$\Delta\lambda_n$	0.5	0.3	1.2	1.0	0.2	0.5
Cr	0.58	0.56	0.58	0.53	0.61	0.56

No outstanding eigenmode(s) can be resolved (e.g., Table 5). On the other hand, the two leading modes from SVD analyses for OLR'_p and U'_{850} and for OLR reconstructed from its first two EOF modes and U'_{850} explain 98% of the total covariance. Therefore, in spite of the different spectral peaks at zonal wavenumbers 1 and 2 for the three reconstructed OLR fields (Figs. 2b, 2c, and 4a), they represent essentially the same intraseasonal component of convection that is coherent with the eastward propagating circulation signals of the MJO.

4. Discussion

The results presented in the previous sections can be summarized as follows.

1) No evidence can be found that unambiguously indicates a dominant intraseasonal standing oscillation in large-scale tropical convection.
2) Both EOF and HSVD analyses of OLR demonstrate that the dominant intraseasonal fluctuation of convection exhibits eastward propagation at wavenumbers 1–3 (referred to as the propagating component), which is confined to the equatorial Indian and western Pacific Oceans. We interpret this propagating component as the convective manifestation of the MJO.
3) This propagating component accounts for most of the variance in convection that is coherent with the dominant eastward propagating mode in the zonal wind, which is a traditional measure of the MJO.
4) There is no coherence between the zonal wind and the remaining OLR after the propagating component has been removed.

A question can thus be raised: Why is an intraseasonal standing oscillation in OLR apparent in time–longitude diagrams (e.g., Fig. 1) and other diagrams but fails to be resolved by these statistical analyses? To address this question, we construct two synthetic time series, $A(\lambda, t)$ and $B(\lambda, t)$, where λ is longitude and t is time in the interval -250 d $< t < +250$ d. Both time series oscillate at an arbitrary period of 50 days and are attenuated with a Gaussian window of the form $\exp[-(t/30$

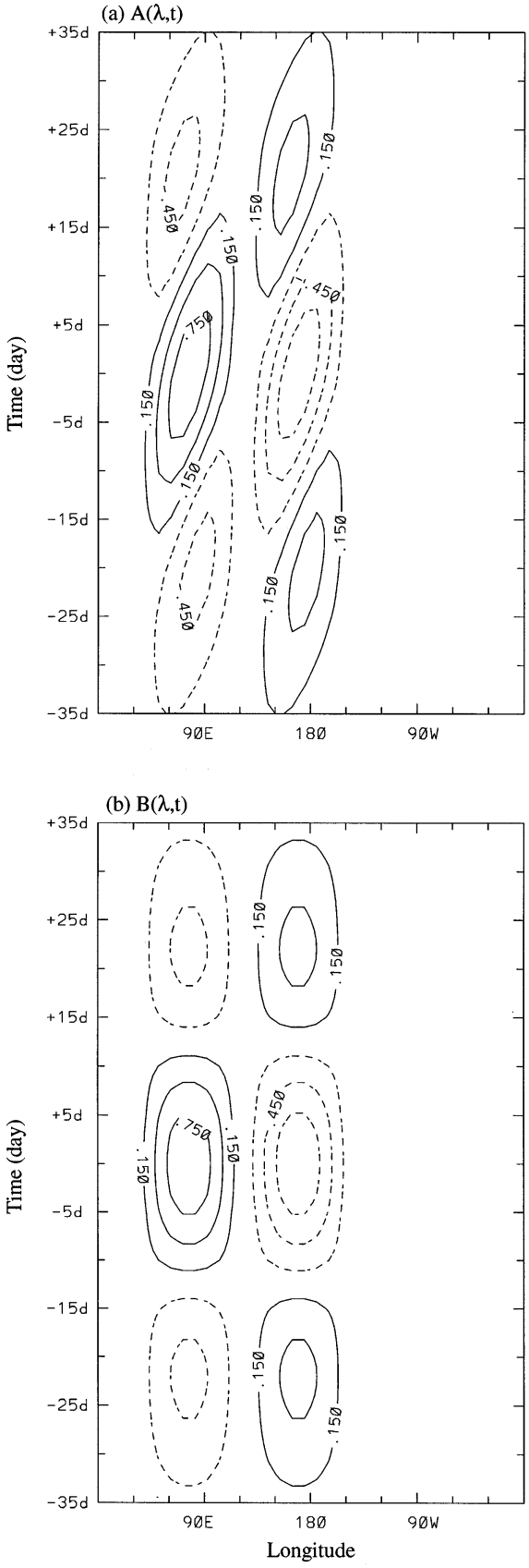

Fig. 6. Time–longitude diagram for synthetic time series (a) $A(\lambda,t)$ and (b) $B(\lambda,t)$. Negative contours are dashed.

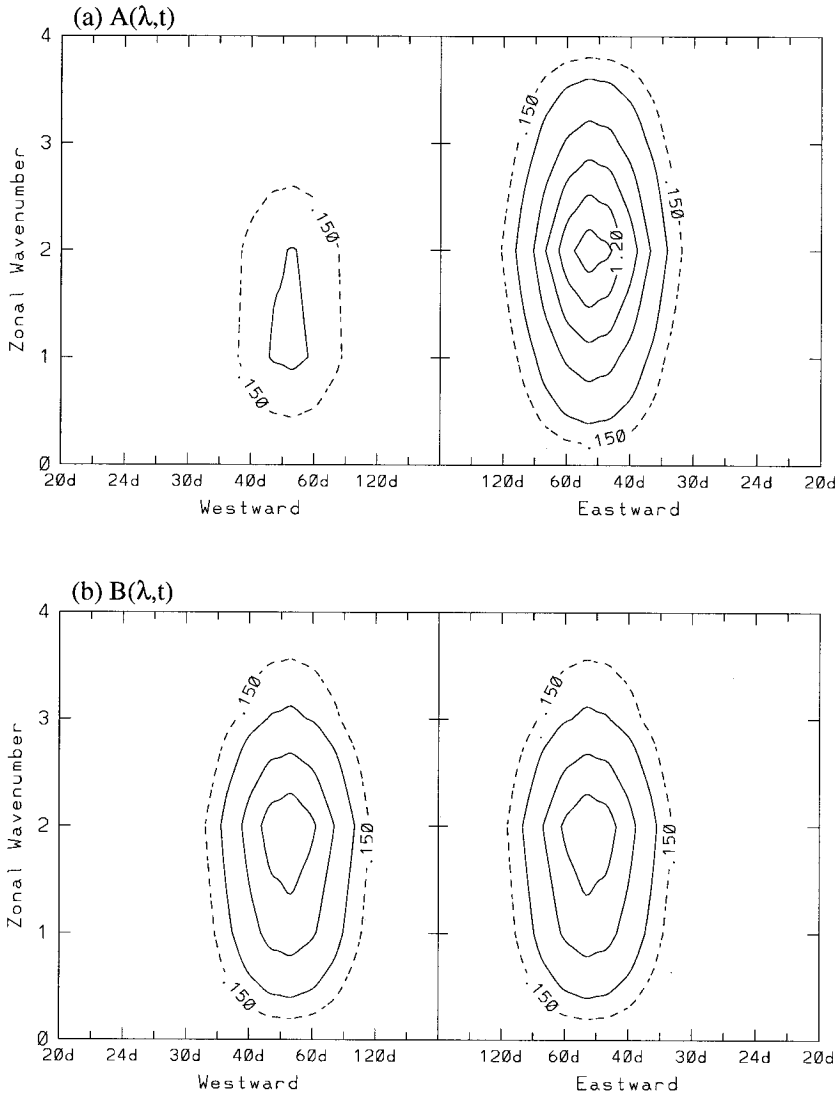

FIG. 7. Space–time power spectra for synthetic time series (a) $A(\lambda, t)$ and (b) $B(\lambda, t)$. The first contour value (dashed) is one-half the solid contours.

d)^2], which acts to broaden the frequency spectrum. This Gaussian window mimics the tendency for the observed signal of the MJO to decorrelate after about one cycle (Hendon and Salby 1994). Both time series consist of zonal wavenumber 2, which is confined approximately from 35°E to 155°W and whose amplitude is modulated by a zonally varying envelope. Their time–longitude variations (Figs. 6a and 6b) show apparent ''seesaw'' patterns, with opposite phases at 75°E and 165°E. One may get an impression that both time series consist of a strong standing oscillation. Their space–time power spectra indicate, however, that $A(\lambda,t)$ possesses dominant eastward power (Fig. 7a) while $B(\lambda,t)$ has equal eastward and westward power (Fig. 7b). In fact, $A(\lambda,t)$ represents an eastward propagating wavenumber 2 disturbance whose amplitude is modulated by the envelope function $F(\lambda)$ with maxima at 75°E and 165°E:

$$A(\lambda, t) = F(\lambda)\exp[-(t/30\text{ d})^2]\exp[2\pi i(k_0\lambda/360^\circ - t/\tau_0)], \quad (3)$$

where $k_0 = 2$, $\tau_0 = 50$ days, t is time in days, λ is longitude in degrees, and

$$F(\lambda) = \begin{cases} \cos\left(\dfrac{\lambda - 75^\circ}{80^\circ}\right), & \text{for } 35^\circ\text{E} < \lambda < 115^\circ\text{E}; \\ \cos\left(\dfrac{\lambda - 165^\circ}{80^\circ}\right), & \text{for } 125^\circ\text{E} < \lambda < 155^\circ\text{W}; \\ 0, & \text{otherwise.} \end{cases} \quad (4)$$

Here, $A(\lambda, t)$ can be regarded as a highly idealized representation of the observed intraseasonal variation of convective activity along the equator. The envelope function $F(\lambda)$ represents the observed longitudinal localization of convective variance over the eastern Indian and western Pacific Oceans (e.g., Salby and Hendon 1994). On the other hand, $B(\lambda, t)$ is a pure standing oscillation of zonal wavenumber 2, whose amplitude is modulated by the same envelope $F(\lambda)$,

$$B(\lambda, t) = F(\lambda)\exp[-(t/30\ d)^2]\exp[2\pi i(k_0\lambda_0/360^\circ - t/\tau_0)], \quad (5)$$

where

$$\lambda_0 = 75^\circ\text{E}.$$

This demonstration, based on synthetic time series, illustrates that a modulation of the eastward propagating large-scale convective disturbance by an amplitude envelope may lead to an impression of a strong standing oscillation. While the amplitude envelope does lead to a spreading of the eastward propagating wavenumber 2 into adjacent eastward wavenumbers and, to a much lesser degree, into adjacent westward wavenumbers, the resulting ratio of eastward to westward powers is comparable to that associated with the total spectrum of OLR (see Fig. 2a) and is actually substantially less than that associated with the MJO (see Fig. 2c). This suggests that the observed signal of convection is not as spatially confined as that of this synthetic time series. Indeed, a weak convective signal is associated with the MJO over equatorial Africa and South America (e.g., Lau and Chan 1988; Salby and Hendon 1994).

The observed amplitude envelope exhibits maxima over the warm water in the eastern Indian and western Pacific Oceans and a minimum over the Maritime Continent (Salby and Hendon 1994). It is an intriguing problem why intraseasonal convective activity is diminished over the Maritime Continent. Although it is beyond the scope of the present study to thoroughly investigate this problem, we propose three possible explanations: (i) the local energy supply by turbulent fluxes from the sea surface is diminished over the land surfaces, (ii) the remote energy supply by large-scale moisture convergence is reduced because the topography interferes with the frictionally induced circulation in the boundary layer, and (iii) convective variability over land is dominated by a vigorous diurnal cycle maintained by various local mechanisms (e.g., sea breezes and land-surface diurnal heating) that are independent of the phase of the MJO.[2]

In conclusion, the results from this study indicate that scenario 2 proposed in section 1, that is, ''the MJO is mainly a phenomenon of eastward propagation in the circulation disturbance induced by localized standing oscillation in convection,'' is not supported by our observations. Mechanisms that emphasize interactions between the propagating components of the circulation and convection are more feasible. Although our analyses are not sufficient to offer a deterministic preference between scenarios 1 and 3, evidence can be found that favors scenario 1 over 3. For example, the spatial distribution of variance associated with the leading modes derived from the HSVD analysis for U'_{850} is essentially the same as that of U^*_{850} shown in Fig. 5a. This implies that outside the region where convection and the circulation are closely coupled, intraseasonal propagating signals in the circulation weaken, for example, in the eastern Pacific. This would be hard to explain if the anomalous circulation was not sustained through its interaction with the eastward propagating component of convection, which loses its local energy supplies and perishes over the cold sea surface in the eastern Pacific. Furthermore, organized convection over the continents of Central and South America and Africa is also very strong, especially in boreal winter. If scenario 3 is operating, we would expect substantial intraseasonal signals in the circulation and convection in the Western Hemisphere. In reality, they are much weaker than those in the Eastern Hemisphere (e.g., Salby and Hendon 1994).

Finally, we emphasize that it is the physics pertinent to the interaction between eastward propagating disturbances in the circulation and convection that are crucial to our understanding of the MJO. Theories and hypotheses postulated to explain the possibility that intraseasonal variability in convection can be promoted by local dynamics and thermodynamics would be more useful if they were placed in the context of explaining the geographical modulation and confinement of the large-scale, eastward propagating convective disturbance.

Acknowledgments. This study was supported by NSF Grant ATM-9320193, the NOAA Office of Global Programs through an award under Cooperative Agreement NA37RJ0198 to JISAO (CZ), and by a TOGA COARE grant from the NOAA Office of Global Programs (HHH). A portion of this work was performed while HHH was attached to the CDC for Southern Hemisphere Meteorology at Monash University, Melbourne, Australia. This is JISAO Contribution Number 211.

REFERENCES

Anderson, J. R., and D. E. Stevens, 1987: The response of the tropical atmosphere to low frequency thermal forcing. *J. Atmos. Sci.,* **44,** 676–686.

Barnett, T. P., 1983: Interaction of the monsoon and Pacific trade wind system at interannual time scales. Part I: The equatorial zone. *Mon. Wea. Rev.*, **111,** 756–773.

Bretherton, C. S., C. Smith, and J. M. Wallace, 1992: An intercomparison of methods for finding coupled patterns in climate data. *J. Climate,* **5,** 541–560.

[2] Wang and Li (1994) have proposed hypotheses similar to scenarios 2 and 3.

Emanuel, K. A., 1987: An air–sea interaction model of intraseasonal oscillations in the Tropics. *J. Atmos. Sci.,* **44,** 2324–2340.

Hayashi, Y., 1979: A generalized method of resolving transient disturbances into standing and traveling waves by space–time spectral analysis. *J. Atmos. Sci.,* **36,** 1017–1029.

——, and D. G. Golder, 1986: Tropical intraseasonal oscillation appearing in the GFDL general circulation model and FGGE data. Part I: Phase propagation. *J. Atmos. Sci.,* **43,** 3058–3067.

Hendon, H. H., and M. L. Salby, 1994: The life cycle of the Madden–Julian oscillation. *J. Atmos. Sci.,* **51,** 2225–2237.

Hsu, H.-H., B. J. Hoskins, and F.-F. Jin, 1990: The 1985/86 intraseasonal oscillation and the role of the extratropics. *J. Atmos. Sci.,* **47,** 823–839.

Hu, Q., and D. A. Randall, 1994: Low-frequency oscillations in radiative–convective systems. *J. Atmos. Sci.,* **51,** 1089–1099.

Knutson, T. R., and K. M. Weickmann, 1987: 30–60 day atmospheric oscillations: Composite life cycles of convection and circulation anomalies. *Mon. Wea. Rev.,* **115,** 1407–1436.

Lau, K. M., and P. H. Chan, 1985: Aspects of the 40–50 day oscillation during the northern winter as inferred from outgoing longwave radiation. *Mon. Wea. Rev.,* **113,** 1889–1909.

——, and L. Peng, 1987: Origin of low-frequency (intraseasonal) oscillations in the tropical atmosphere. Part I: Basic theory. *J. Atmos. Sci.,* **44,** 950–972.

——, and ——, 1988: Intraseasonal and interannual variations of tropical convection: A possible link between the 40–50 day oscillation and ENSO? *J. Atmos. Sci.,* **45,** 506–521.

Madden, R. A., and P. R. Julian, 1971: Detection of a 40–50 day oscillation in the zonal wind in the tropical Pacific. *J. Atmos. Sci.,* **28,** 702–708.

——, and ——, 1972: Description of global-scale circulation cells in the tropics with a 40–50 day period. *J. Atmos. Sci.,* **29,** 1109–1123.

Nakazawa, T., 1986: Mean features of 30–60 day variations as inferred from 8-year OLR data. *J. Meteor. Soc. Japan,* **64,** 777–786.

Neelin, J. D., I. M. Held, and K. H. Cook, 1987: Evaporation–wind feedback and low-frequency variability in the tropical atmosphere. *J. Atmos. Sci.,* **44,** 2341–2348.

North, G. R., T. L. Bell, R. F. Cahalan, and F. J. Moeng, 1982: Sampling errors in the estimation of empirical orthogonal function. *Mon. Wea. Rev.,* **110,** 699–706.

Pratt, R. W., 1976: The interpretation of space–time spectral quantities. *J. Atmos. Sci.,* **33,** 1060–1066.

Rui, H., and B. Wang, 1990: Development characteristics and dynamic structure of tropical intraseasonal convection anomalies. *J. Atmos. Sci.,* **47,** 357–379.

Salby, M. L., and R. R. Garcia, 1987: Transient response to localized episodic heating in the Tropics. Part I: Excitation and short-time, near-field behavior. *J. Atmos. Sci.,* **44,** 458–498.

——, and H. H. Hendon, 1994: Intraseasonal behavior of clouds, temperature, and motion in the Tropics. *J. Atmos. Sci.,* **51,** 2207–2224.

——, R. R. Garcia, and H. H. Hendon, 1994: Planetary-scale circulations in the presence of climatological and wave-induced heating. *J. Atmos. Sci.,* **51,** 2344–2367.

Wallace, J. M., C. Smith, and C. S. Bretherton, 1992: Singular value decomposition of wintertime sea surface temperature and 500-mb height anomalies. *J. Climate,* **5,** 561–576.

Wang, B., 1988: Dynamics of tropical low-frequency waves: An analysis of the moist Kelvin wave. *J. Atmos. Sci.,* **45,** 2051–2065.

——, and T. Li, 1994: Convective interaction with boundary-layer dynamics in the development of a tropical intraseasonal system. *J. Atmos. Sci.,* **51,** 1386–1400.

Weickmann, K. M., and S. J. S. Khalsa, 1990: The shift of convection from the Indian Ocean to the western Pacific Ocean during a 30–60 day oscillation. *Mon. Wea. Rev.,* **118,** 964–978.

——, G. R. Lussky, and J. E. Kutzbach, 1985: Intraseasonal (30–60 day) fluctuations of outgoing longwave radiation and 250 mb streamfunction during northern winter. *Mon. Wea. Rev.,* **113,** 941–961.

Yamagata, T., and Y. Hayashi, 1984: A simple diagnostic model for the 30–50 day oscillation in the Tropics. *J. Meteor. Soc. Japan,* **62,** 709–717.

Zhu, B., and B. Wang, 1993: The 30–60-day convection seesaw between the tropical Indian and western Pacific Oceans. *J. Atmos. Sci.,* **50,** 184–199.